Ligand content and driving force effects on ion-ion permselectivity in ligand-functionalized membranes

Kristen Abels[a], Amilton Barbosa Botelho Junior[a], Xi Chen[b], William A. Tarpeh[a*]

[a]*Department of Chemical Engineering, Stanford University, Stanford, California 94305, United States*

[b]*School of Energy and Environment, City University of Hong Kong, Kowloon, Hong Kong SAR.*

* Corresponding author: email: wtarpeh@stanford.edu

Abstract

Ion-selective membranes could enable sustainable critical material separations processes because of their scalability, low energy consumption, and low chemical input. The effects of membrane water content and incorporation of ion-coordinating ligands have been studied via computation and experiment to develop structure-performance relationships. However, few studies systematically investigate the effects of membrane composition beyond monomer chemical identity or the balance of driving forces such as diffusion and electromigration. Here we synthesized a library of poly(ethylene glycol) acrylate membranes with varying percentages of ion-coordinating monomers (acrylic acid, 4-vinylpyridine) to investigate the influence of ligand content on ion permeabilities and permselectivities. Trends in membrane performance under electrodialysis and diffusion were compared to elucidate the relative effects of separation driving forces and to inform electrochemical operation. We observed order-of-magnitude permeability reductions with ligand content for ions capable of multidentate ligand complexation, especially for nickel in the pyridine-containing membranes. As a result, lithium/nickel permselectivity gradually increased by a factor of 1.65× from 10 to 50 mol% pyridine membranes. We further demonstrated simultaneous improvements in lithium/nickel separation productivity (1.75×) and selectivity (2.99×) with increasing electric potential driving force. Ultimately, results from this study provide design insights for ligand-functionalized membranes in electrified ion-ion separations processes.

Keywords

Electrodialysis; ion-ligand affinity; lithium separation; partitioning; selective transport

Graphical Abstract

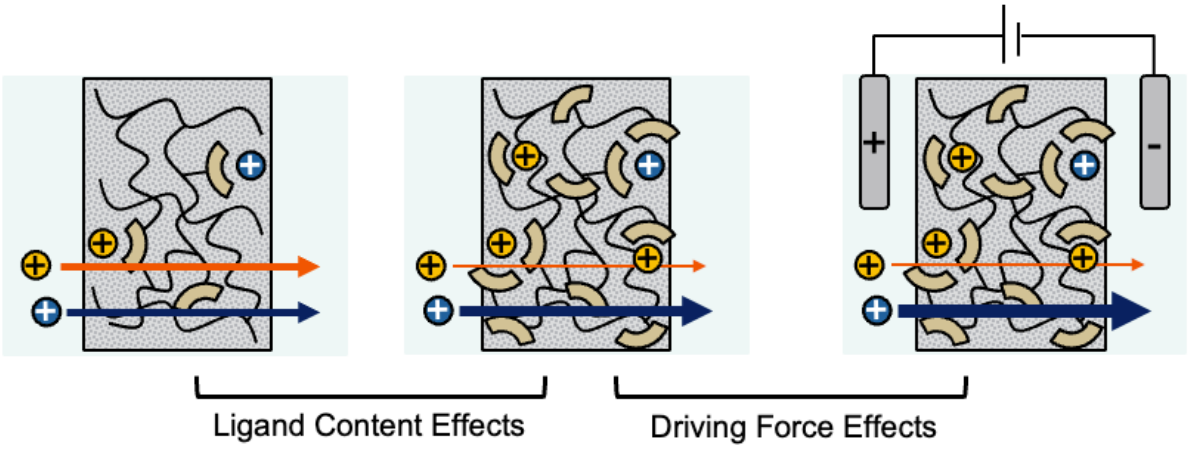

1 Introduction

The exponential growth in demand for lithium exemplifies the need for novel ion-selective separations processes [1,2]. With global lithium supplies projected to fall short of demand by 2030, there is great incentive to develop new technologies to recover lithium from alternative sources such as lithium-ion battery waste and oilfield brines [2–4]. Both waste streams require selective separations for high-purity direct lithium extraction due to the presence of other cations. To achieve efficient selective recovery of critical raw materials like lithium from complex solutions, new separation processes and materials (e.g., organic solvents, adsorbents, membranes) are required [1].

Membrane-based separation processes offer the advantages of scalability, continuous operation, low energy consumption, and low chemical input [5–7]. While reverse osmosis and electrodialysis processes are well-established for efficient water-salt separation, highly selective ion-ion separations remain largely infeasible with commercial polymeric membrane materials [8–10]. Existing membranes leverage differences in size, charge, and valence for selectivity, but often cannot distinguish between ions with similar properties [11]. Introducing coordinating ligands for ion-specific interactions may facilitate the selective permeation of one ion over others by enhancing that ion's partitioning into the membrane; however, strong ion-ligand interactions may also reduce an ion's mobility within the membrane, resulting in retention rather than permeation [12,13]. These opposing effects of ion-ligand interactions on ion partitioning and ion mobility currently preclude *a priori* prediction of ion permselectivity in ligand-functionalized membranes.

Two contrasting results have emerged in literature; in some cases, researchers have observed permselectivity for the ion with strongest ligand affinity [12,14–17], whereas others have observed reverse permselectivity of the ion with lower ligand affinity [13,18,19]. As an example of the former, novel imidazole-containing polymeric membranes offered copper cation permselectivity compared to competing divalent cations due to the higher affinity of copper cations to imidazole groups [14,15]. A contrasting example of strong ligand affinity leading to reverse selectivity was shown for lithium/sodium separations with 12-crown-4-ether-functionalized membranes. In this case, lithium/sodium permselectivity was attributed to stronger sodium-ligand interactions compared to lithium-ligand interactions [20]. Subsequent molecular dynamic simulations supported the alternative conclusion that strong cation-ligand interactions hinder ion mobility to a greater extent than they enhance partitioning, resulting in the overall reduction in ion permeability with increasing interaction strength [13]. These experimental and molecular dynamic simulation studies have been complemented with transport theory that predicts membrane permselectivity

as a function of ion and membrane properties such as valence, concentration, ion exchange capacity, fractional water content, and ion-ligand coordination free energy [21,22].

While dependencies of ion transport on ion valence, membrane fractional water content, and ion exchange capacity have been thoroughly investigated experimentally [8,23,24], trends with ion-ligand coordination affinity are rare despite its clear importance as a governing factor in ion transport [10,11]. We aim to fill this gap in experimental studies by systematically assessing ion-ligand coordination affinity as a predictor for ion transport. Ion-ligand coordination affinity is customarily tuned through ligand selection; however, we hypothesize that ligand content within a confined membrane environment can also influence ion-ligand coordination interactions, especially in the case of multidentate interactions. Steric hindrance resulting from ligand attachment to the polymer backbone is expected to severely limit the occurrence of strong multidentate interactions, especially at low ligand contents for which the probability of adjacent ligands on the random copolymer backbone is low [25]. We therefore postulate that membrane ligand content, a previously understudied parameter, may exhibit substantial, measurable impacts on ion-membrane affinities and ion transport [9].

Although membrane performance is often studied under diffusive transport conditions, realistic implementation of membrane-based ion-ion separations likely requires an enhanced driving force beyond concentration gradient, such as pressure or electric potential, to reach industrially-relevant fluxes. Thus, informed membrane-based electrochemical separations require consideration of the interplay of ion-membrane affinity and driving force in ligand-functionalized membrane performance. In this work, we focus on the effect of additional electric potential driving force present in selective electrodialysis – a process that has previously been investigated for battery recycling and aligns well with the National Academies electrification goals for sustainable separations [26,27]. A common concern in the membrane community is that valence-proportional electromigratory flux from an electric potential driving force may drastically impair ion-ion permselectivity in the separation of ions of different valence (e.g., lithium/nickel separation) [28]. It is therefore worth investigating whether permselectivities afforded by ligand-functionalized membranes under diffusion experiments can be maintained in selective electrodialysis [9].

Overall, this study aims to elucidate the relationships between design parameters (ion-ligand affinity, ligand content, and driving force) and ion transport performance (ion sorption, ion permeability, and ion-ion permselectivity). To this end, we synthesized a library of ligand-functionalized membranes and systematically compared ion permeability and selectivity. Model feedstocks consisting of lithium and competing ions of sodium and magnesium were motivated by the industrial interest for lithium recovery from produced water brines, while a model feedstock containing lithium and nickel was motivated by

lithium recovery from battery waste. The library of poly(ethylene glycol) acrylate membranes includes two ligands (carboxylic acid, pyridine) tested separately at monomer contents of 0-50 mol%. Testing all membranes for the separation of the three ion pairings (Li^+/Na^+, Li^+/Mg^{2+}, Li^+/Ni^{2+}) represented a systematic experimental matrix for the controlled study of the effects of (1) ligand identity and (2) ligand content on ion transport. These two parameters ultimately impact effective ion-membrane affinity, which in turn influences ion permeability. The additional study of ion-ion separation in one of the novel ligand-functionalized membranes under diffusion versus electrodialysis provided additional information on the interplay of binding energy and driving force in ligand-functionalized membrane performance. Together, the results of this work provide evidence that ligand content and operating conditions are critical considerations in the design of polymeric membrane separation processes for effective ion-ion separations. The systematic data set from this study can help guide more extensive theoretical ion transport model development and refine membrane design rules.

2 Experimental

2.1 Membrane synthesis

Photopolymerization was used to fabricate eleven hydrogel membranes containing poly(ethylene glycol) methyl ether acrylate (PEGMEA, M_n 480), poly(ethylene glycol) diacrylate crosslinker (PEGDA, M_n 700), and 0 to 50 mol% of one of two ion-coordinating monomers: acrylic acid (AA, ≥ 99.0 %, stabilized with hydroquinone monomethyl ether for synthesis) or 4-vinylpyridine (4VP, 95% stabilized with 100 ppm hydroquinone) [29–32]. All monomer precursors were purchased from Millipore Sigma; AA and 4VP were chosen because of their span of affinities across several cations (Table S1). Solvent-free mixtures of PEGMA, PEGDA, and the ligand-containing monomer (purified by single pass through alumina-based inhibitor removers (Sigma-Aldrich)) were prepared based on desired monomer compositions (Table 1). Following photoinitiator addition (2,2-dimethoxy-2-phenylacetophenone, 99%, Millipore Sigma), the pre-polymer mixtures were sonicated to remove air bubbles and cast between 4"×4" quartz plates (Flinn Scientific) with 0.5 mm silicone rubber spacers (LMS). Polymer films were irradiated with 365 nm UV light (DarkBeam A300 LED Flashlight) for 20-40 minutes and cut to 10 mm and 16 mm diameter membrane coupons using a hollow punch set (J&D Jindiao).

2.2 Characterization of membrane structural properties

Polymer gel fractions were determined via dialysis with 2-methyltetrahydrofuran (MeTHF, Honeywell) following previously reported methods [33,34]. Briefly, 10 mm diameter coupons were soaked in MeTHF for two days and dried overnight at 50 °C in a vacuum oven (Across International). Gel fractions were calculated as the ratio of dry mass of the sample after (m_{dia}) and before dialysis (m_{dry}): m_{dia}/m_{dry}. Qualitative trends in membrane ligand content were analyzed using attenuated total reflectance Fourier transform infrared spectroscopy (ATR-FTIR) with a Nicolet iS50 FT/IR Spectrometer. Triplicate ATR-FTIR measurements were taken from different membrane samples, indiscriminate of surface side, to best quantify membrane homogeneity.

Membrane water uptake was measured by soaking 16 mm diameter coupons in nanopure water (18.2 MΩ·cm resistivity) for 24 hours. Hydrated membrane mass (m_w) was measured after careful removal of residual water on the membrane surface with a KimWipe [34]. Corresponding dry membrane mass (m_{dry}) was measured after drying in a vacuum oven overnight at 50 °C. The difference in hydrated and dry membrane mass relative to dry mass gives the water uptake : $WU = (m_w - m_{dry})/m_{dry} \times 100\%$ [29]. Fractional water content (ϕ_w) was calculated based on membrane water uptake, water density ($\rho_w \approx 1$ g/mL), and dry

polymer density (ρ_p) assuming volume additivity: $\phi_w = WU \times (WU + \rho_w / \rho_p)^{-1}$ [20,35,36]. Dry polymer density was calculated from dry membrane mass and dimensions (Mitutoyo micrometer).

2.3 Ion sorption, permeability, and ion-ion permselectivities

Single- and binary-salt solutions for use in sorption and permeability experiments were prepared by dissolving 100 mM lithium chloride (LiCl, Sigma), sodium chloride (NaCl, Sigma), magnesium chloride hexahydrate (≥ 99.0% $MgCl_2 \cdot 6H_2O$, Millipore Sigma), and/or nickel chloride hexahydrate ($NiCl_2 \cdot 6H_2O$, Sigma) in nanopure water.

Lithium sorption selectivities versus sodium, magnesium, and nickel were measured by soaking 10 mm diameter membrane coupons in 10 mL of binary-salt solutions for 48 h to achieve salt partitioning equilibrium (Fig. S1). The equilibrium solutions were sampled prior to transferring the equilibrated membranes to 10 mL of 5 M nitric acid (prepared from Fisher Scientific 67-70% TraceMetal™ grade nitric acid) for desorption. Desorption solutions were sampled after 24 h, and the desorption process was repeated a second time in 8 mL of 5 M nitric acid. Ion concentrations in the sorption (C_X^S) and desorption (C_X^D) solutions were quantified via ICP-OES (Thermo Scientific ICAP 6300 Duo View Spectrometer). Along with the desorption solution volume (V_D) and the hydrated membrane mass (m_w), these concentration measurements were used to calculate cation uptake ($(\Sigma_i C_{X_i}^D V_{D_i})/m_w$, measured in mmol/g hydrated membrane mass) and lithium partitioning selectivities:

$$S_{X/Y}^{\alpha} = \frac{\left(\Sigma_i C_{X_i}^D V_{D_i}\right)}{\left(\Sigma_i C_{Y_i}^D V_{D_i}\right)} \frac{C_Y^S}{C_X^S} \quad \text{(Eq 1)}$$

Cation permeabilities were measured in diffusion experiments with single-salt or binary-salt feed solutions and nanopure water permeate solutions in custom H-cells 3D-printed from an epoxy polyacrylate photopolymer resin (Fig. S2). In each experiment, a 16 mm diameter membrane pre-hydrated in nanopure water was clamped between 40 mL feed and permeate chambers with an effective cross-sectional area of $A_m = 1.77$ cm^2. Feed and permeate chamber solutions were continuously stirred, and cation concentrations were monitored via ion chromatography. Cation chromatography (4 mM tartaric acid/2 mM oxalic acid eluent, SCS 1 column at 30 °C) was performed with a dual Dionex ICS-6000 system. The steady-state rate of change of permeate ion concentration over time ($\frac{dC_i^P}{dt}$) was used to calculate ion flux (mmol·m^{-2}·h^{-1}), assuming constant permeate chamber volume (V_P) over the course of the experiment (negligible water diffusion and sampling effects):

$$J_i = \left(\frac{dC_i^P}{dt}\right)\frac{V_P}{A_m} \quad \text{(Eq 2)}$$

Normalization of ion flux by the concentration gradient yields ion permeability ($cm^2 \cdot s^{-1}$):

$$P_i = J_i \left(\frac{C_i^F}{l}\right)^{-1} \quad \text{(Eq 3)}$$

In the calculation of permeability, the concentration gradient is approximated by initial feed concentration (C_i^F) divided by membrane thickness (l) [29]. The diffusion experiments ranged from 4 to 144 hours in duration to ensure a steady-state flux measurement. The longer duration experiments were required to measure post-breakthrough permeability of nickel in the pyridine-containing membranes (Fig. S3). In the diffusion experiments with binary-salt feed solutions, ion-ion permselectivities of cation X over cation Y were calculated as the ratio of their respective permeabilities:

$$S_{X/Y} = \frac{P_X}{P_Y} \quad \text{(Eq 4)}$$

Electrodialysis studies of lithium/nickel permselectivity were performed for the 50 mol% pyridine-containing membrane. A custom 4-chamber cell stack was used in these experiments consisting of 20 mL anode, feed, permeate, and cathode chambers (Fig. S4). The 50 mol% pyridine-containing test membrane was clamped between the feed and permeate chambers following equilibration in the feed solution (binary-salt solution of 100 mM LiCl and 100 mM $NiCl_2$). A 0.1 M sulfuric acid (H_2SO4) solution was used in all other chambers. Quaternary ammonium-functionalized AXM-100 anion-exchange membranes (Membranes International Inc.) equilibrated in 0.1 M H_2SO4 were clamped between the anode and feed chambers as well as the permeate and cathode chambers to mitigate cation migration into the anolyte and catholyte. An iridium MMO-coated titanium mesh anode (2 × 2 cm, Optimum Anode Technologies) and platinum wire cathode (5 cm × 0.5 mm diameter, BASi Inc.) were used with a BioLogic VMP-300 potentiostat to achieve applied stack voltages of 2.8, 5.0, and 6.5 V. Feed and permeate solutions were recirculated at 22 mL/min via peristaltic pump (Masterflex), and compositions were monitored over 24 hours via ICP-OES to track ion flux and lithium permselectivity. Due to unsteady-state behavior over the course of the chronoamperometry experiments, steady-state permeabilities and permselectivities could not be calculated in the same manner as the diffusion experiments. Instead, the ratio of average lithium and nickel concentrations in the permeate chamber ($C_{i,}^P(t)$), normalized by the initial concentrations in the feed chamber ($C_i^F(0)$), were calculated at each sampling timepoint to give a proxy for the time-averaged permselectivity up to that timepoint:

$$S^{*}_{X/Y}(t) = \frac{C^{P}_{Li}(t)}{C^{P}_{Ni}(t)} \cdot \frac{C^{F}_{Ni}(0)}{C^{F}_{Li}(0)} \quad \text{(Eq 5)}$$

3 Results and Discussion

Following synthesis and physicochemical characterization of our membrane library (Section 3.1), we performed single-salt diffusion experiments to assess the impact of ligand identity (Section 3.2.1) and ligand content (Section 3.2.2) on ion permeability. Subsequent binary-salt diffusion and partitioning experiments provide insights for ligand content effects on ion-ion permselectivity and the primary mechanisms conferring this permselectivity (Section 3.3). Finally, assessment of the performance of one membrane for lithium/nickel separation under diffusion versus electrodialysis enabled further study of driving force effects on permselectivity in ligand-functionalized membranes (Section 3.4).

3.1 Physicochemical properties of ligand-functionalized membranes

Gel fractions exceeding 95% confirm successful polymerization across all membranes (Table 1). ATR-FTIR provided qualitative verification of successful polymerization of the target ligand-functionalized monomer at 10 mol% increments up to a maximal ligand monomer content of 50 mol% (Fig. 1). All membranes share a similar backbone chemistry (Fig. 1A) shown by the common FTIR absorbance spectra (Fig. 1B), where slight variations in absorbance peaks associated with the carboxylic acid or pyridine ligand functional groups confirm the incremental ligand content across membranes (Fig. 1C). Crosslinker concentrations were tuned to maintain constant fractional water content (ϕ_w = 0.47 ± 0.01 SD) across all membranes, and silicone spacers were used during photopolymerization to ensure constant membrane thickness (566 ± 16 μm dry) such that ligand species and ligand content would be the primary variables affecting performance trends [29]. Full characterization details for membrane gel fraction, dry and hydrated thickness, water uptake, and fractional water content are provided in Table 1.

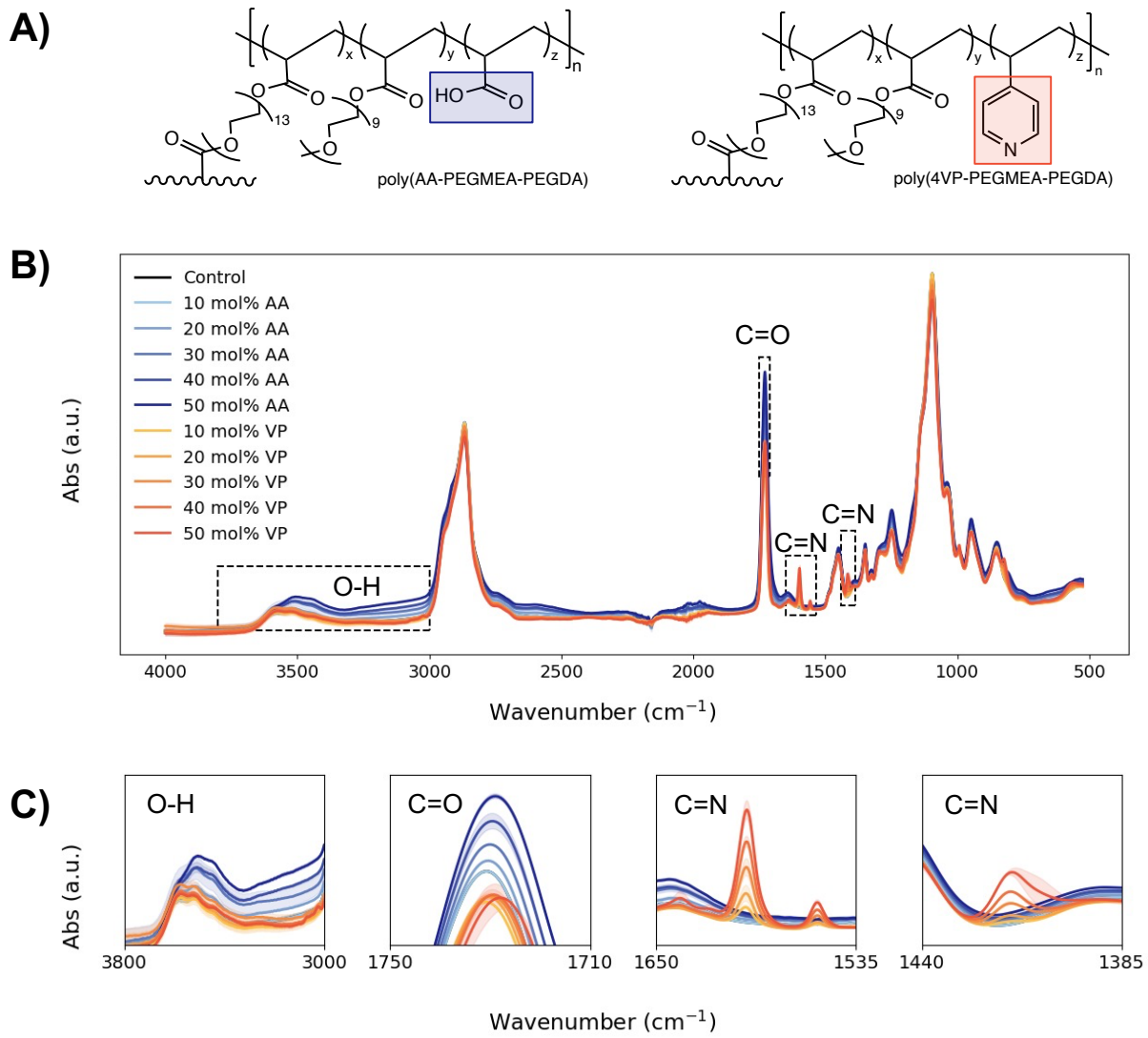

Fig. 1. A) Chemical structures of ligand-functionalized membrane synthesized via photopolymerization. The left structure depicts the carboxylic acid-functionalized membranes, poly(AA-PEGMEA-PEGDA), synthesized using acrylic acid (AA) co-monomer along with poly(ethylene glycol) methyl ether acrylate (PEGMEA) and poly(ethylene glycol) diacrylate (PEGDA). The right structure depicts the pyridine-functionalized membranes synthesized with 4-vinylpyridine (VP) co-monomer (poly(4VP-PEGMEA-PEGDA)). B) ATR-FTIR spectra demonstrating common membrane structures across the entire membrane library, with C) insets of regions of interest providing semi-quantitative confirmation of increasing carboxylic acid (O-H, C=O bond) and pyridine (C=N bond) content across the 10-50 mol% acrylic acid (AA) and 4-vinylprydine (VP) membranes.

Table 1. Physicochemical properties of synthesized ligand-functionalized membranes, including monomer molar composition (AA = acrylic acid, 4VP = 4-vinylpyridine, PEGMEA = poly(ethylene glycol) methyl ether acrylate, PEGDA = poly(ethylene glycol) diacrylate), gel fraction, dry and hydrated thicknesses, water uptake, and water volume fraction. Values are reported as average value ± one standard deviation of triplicate measurements from distinct replicate membranes.

ID	Molar Composition (AA or 4VP /PEGMEA/PEGDA)	Gel Fraction (GF)	Dry Thickness (μm)	Hydrated Thickness (μm)	Water Uptake (WU)	Fractional water content (ϕ_w)
Control	0/50/50	95.8% ± 1.0%	553 ± 6	671 ± 19	78.7% ± 2.1%	0.477 ± 0.004
AA10	10/44/46	95.8% ± 0.7%	596 ± 22	647 ± 3	78.5% ± 1.1%	0.466 ± 0.017
AA20	20/38/42	95.6% ± 1.0%	567 ± 16	658 ± 9	78.1% ± 0.3%	0.475 ± 0.007
AA30	30/32/38	95.2% ± 1.1%	557 ± 30	646 ± 9	74.7% ± 3.2%	0.468 ± 0.016
AA40	40/26/34	95.3% ± 1.3%	539 ± 14	633 ± 18	74.9% ± 1.1%	0.475 ± 0.013
AA50	50/20/30	95.1% ± 1.3%	561 ± 8	649 ± 12	70.2% ± 1.9%	0.462 ± 0.008
4VP10	10/45/45	97.2% ± 0.8%	587 ± 13	663 ± 14	66.3% ± 1.4%	0.476 ± 0.007
4VP20	20/40/40	96.6% ± 0.3%	558 ± 15	665 ± 24	66.5% ± 2.4%	0.494 ± 0.009
4VP30	30/30/40	96.5% ± 0.5%	561 ± 13	656 ± 4	65.6% ± 0.4%	0.490 ± 0.006
4VP40	40/22/38	96.3% ± 0.9%	568 ± 13	646 ± 13	64.6% ± 1.3%	0.462 ± 0.010
4VP50	50/15/35	95.7% ± 1.8%	578 ± 3	671 ± 21	67.1% ± 2.1%	0.451 ± 0.016
Average		95.9% ± 0.7%	566 ± 16	655 ± 12	71.4% ± 5.7%	0.472 ± 0.012

3.2 Influences of ligand identity and content on ion permeability

3.2.1 Ligand identity effects on ion transport

Even at constant fractional water content, ligand identity can have significant effects on ion permeability due to the effect of ion-ligand interactions on ion transport [12,13]. We first compare ion transport within and across three membranes (Fig. 2) – the ligand-free control membrane, the 50 mol% acrylic acid membrane (50 mol% AA), and the 50 mol% 4-vinylpyridine membrane (50 mol% VP) – and we comment on the overall trends in permeability versus ion-ligand interaction strength based on ion-ligand affinities reported in literature (Table S1). Full analysis of statistically significant differences in ion permeabilities within and across membranes are presented in Fig. S5 and Tables S2 and S3 based on the post-hoc Fisher least significant difference (LSD).

In the ligand-free control membrane, minimal ion-specific interactions were anticipated between the cations and the ether oxygens in the polymer sidechains based on prior studies using similar poly(ethylene glycol)-containing monomers as the non-selective structural components of polymer backbone [29,32]. In the absence of strong, specific ion-ligand coordinative interactions, ion permeabilities were therefore expected to depend mainly on ion diffusivities (a function of hydrated radii) and weaker, valence-dependent ion-dipole electrostatic interactions. These size- and valence-dependent effects are consistent with the lower permeabilities ($p < 0.05$) measured for the divalent ions (Ni^{2+}, Mg^{2+}) compared to the monovalent ions (Li^{+}, Na^{+}) (Fig. 2). Specifically, divalent ions may have experienced slightly larger transport hindrance than monovalent ions due to slightly stronger electrostatic interactions with the ether oxygens and lower diffusivities arising from their larger hydrated radii [37,38]. Even still, all measured cation permeabilities in the ligand-free control membrane remain within a factor of two of each other, further supporting prior claims that size- and valence-effects do not confer substantial ion-specific selectivity [11].

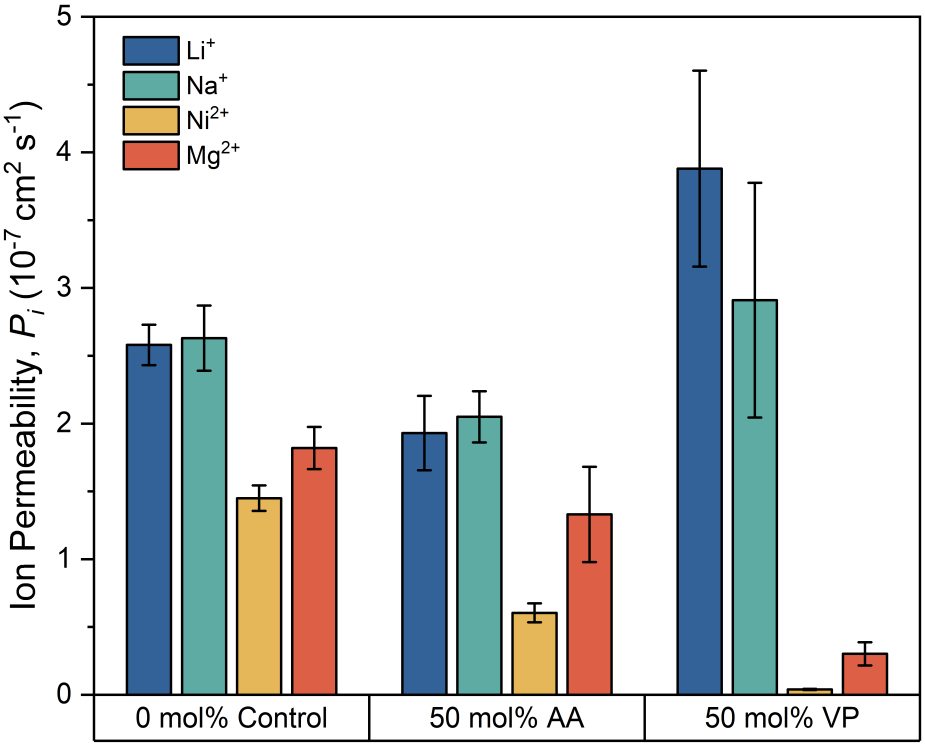

Fig. 2. Diffusive ion permeabilities for lithium (Li^{+}), sodium (Na^{+}), magnesium (Mg^{2+}), and nickel (Ni^{2+}), in the ligand-free control membrane (0 mol% Control) compared to the 50 mol % acrylic-acid (AA) and 50 mol % 4-vinylpryidine (VP) membranes. For example, the leftmost bar in the Fig. shows a lithium permeability of $2.6 \pm 0.1 \times 10^{-7}$ cm^2 s^{-1} in the 0 mol% control membrane. Error bars indicate ± one standard deviation from triplicate experiments, each using new membranes.

Compared to the ligand-free control membrane, ion permeabilities in the 50 mol% acrylic acid membrane (50 mol% AA) are 22-27% lower for Li^+, Na^+, and Mg^{2+}, and 58% lower for Ni^{2+}. Slightly stronger ion-ion electrostatic interactions between the cations and carboxylic acid ligand likely lead to the reductions in permeability for all of the ions studied (statistically significant for Li^+ and Ni^{2+} at $p < 0.05$ and $p < 0.01$, respectively). Comparing between ions in the 50 mol% AA membrane, permeabilities generally follow an inverse trend with ion-carboxylic acid interaction strength (Table S1). Namely, Na^+ and Li^+ have the weakest reported interactions with carboxylic acid moieties and the highest permeabilities, followed by Mg^{2+} (lower than Na^+ at $p < 0.05$), and then Ni^{2+} (lower than Li^+ and Na^+ at $p < 0.001$, and Mg^{2+} at $p < 0.05$). The significantly lower Mg^{2+} and Ni^{2+} permeabilities compared to the other ions are likely due to the ability of these ions to form stronger multidentate coordination complexes with multiple carboxylic acid moieties [39,40]. The cause of this ligand interaction-dependent transport hinderance (e.g., partitioning versus mobility effects) is further investigated in Section 3.3 with subsequent partitioning and permselectivity experiments. Broadly, these preliminary ion permeability results are in agreement with prior reports of permeability reductions in ion permeation due to strong ion-ligand interactions within the membrane [12,13]. Despite the slight differences in carboxylic acid interaction strength with each of the ions (Table S1), the 50 mol% AA membrane still does not effectively discern between the ions as evidenced by their permeabilities which still remain within the same order of magnitude [38].

The 50 mol% 4-vinylpyridine membrane (50 mol% VP) was synthesized to offer a broader range of ion-ligand interaction strengths for the ions of interest, including a much stronger interaction with Ni^{2+} [41,42]. Relative to the ligand-free control membrane, Na^+ and Li^+ permeabilities increased by 10% and 50%, while Mg^{2+} and Ni^{2+} permeabilities decreased by 83% and 97%, respectively. These changes in ion permeabilities between the ligand-free control and 50 mol% VP membranes were statistically significant for Li^+, Mg^{2+}, and Ni^{2+} ($p < 0.001$). The two-order of magnitude span of ion permeabilities in the 50 mol% VP membrane is again attributed to the range of ion-pyridine interaction strengths. The coordinative nickel-pyridine binding affinity far exceeds the pyridine binding affinities towards the other ions in this study (Table S1) [41,42]. While the difference between Mg^{2+} and Ni^{2+} permeabilities in the 50 mol% VP membrane was not identified as statistically significant by the Fisher LSD test, experimental observations did suggest that the transport of Mg^{2+} was not impacted to the same extent as that of nickel due to ion-specific ligand interaction strengths; specifically, nickel transport in the pyridine-containing membrane was found to exhibit a sorption stage prior to breakthrough where nickel transport from feed to permeate was below the limit of detection (SI section S3.1), necessitating longer diffusion experiments for accurate measurement of steady-state permeability post-breakthrough (Fig. S3).

Combined with the ligand-free and 50 mol% AA membranes, these trends in ion permeability again provide additional experimental evidence that ligand identity can be used to tune ion permeabilities. Specifically, we observed the general trend that lower ion permeabilities are associated with strong ion-ligand interactions. Among other possible membrane modifications (e.g., ion exchange capacity, fractional water content), ligand identity modifications are significant and can be more ion-specific. For example, the reduction in post-breakthrough nickel permeability due to pyridine incorporation into the membrane is approximately an order of magnitude higher than reductions in ion permeability reported elsewhere from decreasing fractional water content [8,24]. In addition, while trends in ion permeability with water content are largely independent of ion identity, the effects of ligand identity are ion-specific. These observations evince the benefits of strong ion-ligand coordination interactions beyond electrostatics to achieve significant ion-specific adjustments in permeability.

3.2.2 Ligand content effects on ion transport

In Section 3.2.1, ion permeabilities showed an inverse relationship with ion-ligand interaction strength based on ion-ligand stability constants and bond dissociation energies reported for homogeneous solutions. While ion-ligand binding affinities reported in homogeneous solutions are insightful for preliminary membrane chemistry design, sterically hindered ion-ligand interactions within a confined membrane environment likely differ substantially from those in solution [25]. Therefore, it may not only be crucial to select an appropriate ligand species (e.g., pyridine), but also an appropriate ligand content with the membrane to achieve the desired ion-ligand interactions and tune permeability.

To assess the impact of membrane ligand content on ion transport, ion permeabilities were measured in a series of carboxylic acid- and pyridine-functionalized membranes with ligand contents ranging from 10-50 mol % (Fig. 3). Across both the carboxylic acid and pyridine-containing membranes, Li^+ and Na^+ permeabilities are relatively independent of ligand content, showing no statistically significant linear relationship for the logarithm of permeability versus ligand content (regression and F-test results presented in Table S4). The only statistically significant relationships between ligand content and ion permeability are measured for Mg^{2+} across the acrylic acid membranes ($p < 0.05$) and Ni^{2+} across both the acrylic acid and pyridine-containing membranes ($p < 0.01$ and $p < 0.001$, respectively). We postulate that the unique ligand-content dependence for Ni^{2+} permeability (and to a lesser extent, Mg^{2+} permeability with acrylic acid) and independence for the other ions (Li^+, Na^+, and Mg^{2+} with pyridine) can be explained by coordination chemistry and steric hindrance effects.

Specifically, nickel is reported to form bidentate and hexadentate complexes in bulk solutions with carboxylic acid and pyridine ligands, respectively [39,42]. Magnesium, a divalent ion, is also expected to

form up to bidentate complexes with carboxylic acid groups, although the overall ion-ligand interaction is weaker with magnesium than with nickel [39,40]. For ligands affixed to a membrane, we expected the probability of multidentate complex formation to increase with ligand content due to increased probability of adjacent ligands on the random copolymer backbone [25]. These higher denticity interactions would enhance the average ion-membrane affinity, leading to the reduction in ion permeability that we observed for ions capable of multidentate interactions with increasing membrane pyridine and carboxylic acid contents. Moreover, the strength of these linear relationships as measured by the absolute value of the correlation coefficient ($0 \leq |r| \leq 1$) aligns with the strength of the multidentate ion-ligand interactions: Mg^{2+}-carboxylic acid ($|r| = 0.61$) < Ni^{2+}-carboxylic acid ($|r| = 0.75$) < Ni^{2+}-pyridine ($|r| = 0.98$) [39,40,42].

In contrast to multidentate ion-ligand complexes, Li^{+}, Na^{+}, and Mg^{2+} (with pyridine) are reported to exhibit monodentate interactions with the ligands in bulk solution. Monodentate interactions are generally weaker than multidentate interactions (Table S1). In addition, the ability for monodentate ion-ligand coordination to occur in a membrane matrix (and, in turn, any transport effects resulting from coordination) is likely less affected by the membrane ligand content because, unlike multidentate complexation, there is no requirement for proximate ligands to interact.

Altogether, these findings suggest that homogeneous ion-ligand affinities are necessary but insufficient predictors of ion transport. In particular, when multidentate ion-ligand coordination chemistry increases the overall ion-ligand interaction strength (e.g., nickel-pyridine, nickel-carboxylic acid, and magnesium-carboxylic acid), ligand content must also be considered. We reason that increased ligand content increases the probability of strong multidentate interactions, and that these stronger ion-ligand interactions influence ion permeability. Therefore, ligand content is an additional parameter beyond ligand identity that can tune ion transport in ligand-functionalized membranes.

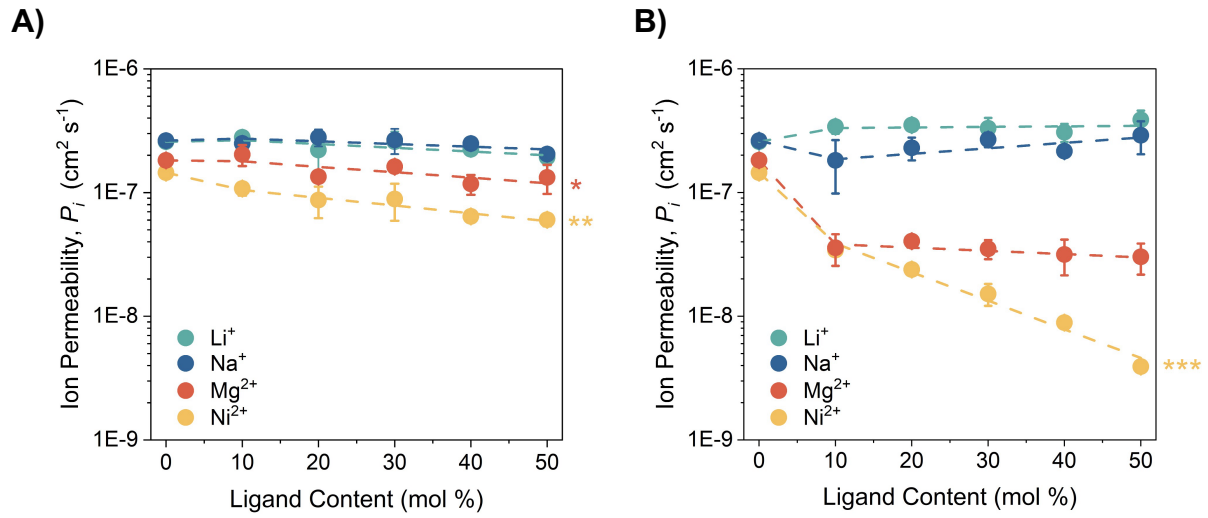

343

344 **Fig. 3. Average ion permeabilities in the A) carboxylic-acid-functionalized and B) pyridine-**
345 **functionalized membranes, plotted against the ligand content (monomer mole percent). Error bars**
346 **represent ± one standard deviation from triplicate experiments. Linear regressions of the logarithm**
347 **of ion permeability with ligand content (10-50 mol%) are shown as dashed lines; statistically**
348 **significant relationships are annotated based on F-tests (* $p \leq 0.05$; ** $p \leq 0.01$; *** $p \leq 0.001$).**

349 ## 3.3 Influences of ligand content on ion-ion permselectivity: mobility effects
350 ## outcompete partitioning effects

351 Because ligand content was observed to impact ion permeability for multidentate-coordinating ions
352 (Ni^{2+}, Mg^{2+}) with negligible effects on monodentate- or weakly-coordinating ions (Li^+, Na^+), we
353 hypothesized that varying ligand content could alter permselectivity between such ion pairs (e.g., Ni^{2+} vs.
354 Li^+). Binary-salt diffusion experiments were performed to test this hypothesis via measurement of ion-ion
355 permselectivities (Fig. 4). In addition, sorption experiments coupled with the solution-diffusion framework
356 were employed to better elucidate the cause of permselectivity trends in ligand functionalized membranes;
357 specifically, partitioning and mobility effects arising from ion-ligand interactions were assessed.

358 We will first discuss permselectivity trends as a function of ligand content, with a focus on the
359 pyridine-containing membranes. The single salt permeability measurements showed a pyridine-content
360 dependence for Ni^{2+} permeability (attributed to increasing probability of strong multidentate coordination),
361 and independence for Li^+, Na^+, and Mg^{2+} permeability (attributed to constant monodentate coordination
362 probability). As a result, Li^+/Ni^{2+} permselectivity was expected to demonstrate a pyridine content
363 dependence, while Li^+/Mg^{2+} and Li^+/Na^+ permselectivities were expected to be independent of pyridine

content. F-tests from linear regression of the logarithm of Li^+/Ni^{2+} permselectivity across the 10-50 mol% pyridine membranes suggest a statistically significant relationship between Li^+/Ni^{2+} permselectivity and ligand content ($p < 0.01$), where permselectivity increased from $S_{Li/Ni} = 7.7 \pm 1.0$ in the 10 monomer mol% pyridine membrane to $S_{Li/Ni} = 12.7 \pm 2.7$ in the 50 mol% membrane (Fig. 4A). Selectivity versus ligand content regression and statistical analyses are reported in Tables S5-S7. Note that these selectivities only account for post-breakthrough transport; the increase in membrane pyridine content from 10 to 50 monomer mol% also extended the nickel sorption period from about $t = 0.1 \pm 0.6$ h to $t = 52 \pm 12$ h in our binary-salt experiments, during which time nickel transport was negligible and an essentially pure lithium product was obtained (Fig. S3). Though not the focus of this work, this selectivity highlights the possibility of employing these materials as absorptive membranes in trace nickel removal applications [43].

Considering the other ion pairs, no significant relationships ($p < 0.05$) between permselectivity and ligand content were identified for Li^+/Na^+ or Li^+/Mg^{2+} (Fig. 4B-C), as expected from the individual ion permeability trends. Similar results were obtained for all salt pairs across the membranes containing acrylic acid, where a statistically significant Li^+/X permselectivity relationship with ligand content was only observed for Li^+/Ni^{2+} ($p < 0.05$) (Fig. S6, Table S5).

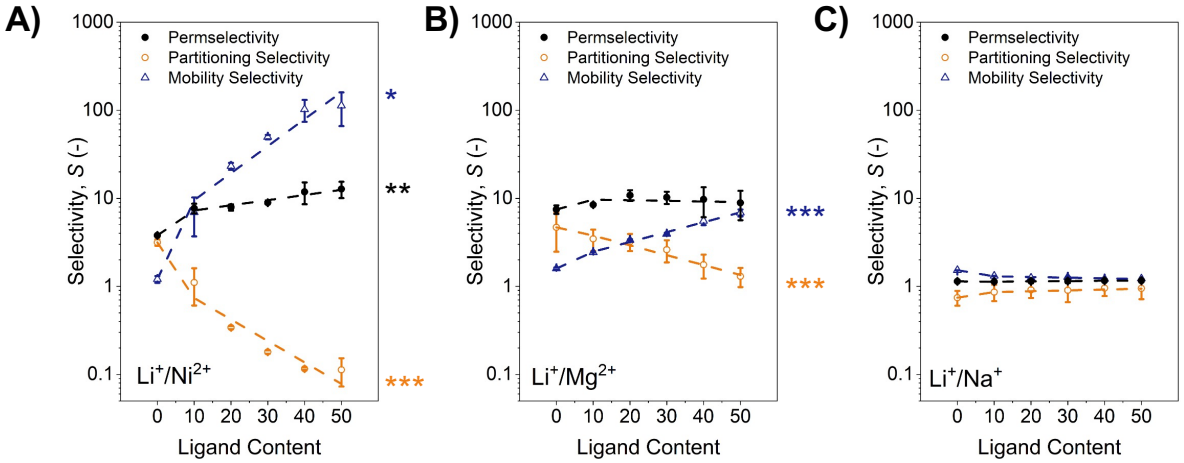

Fig. 4. Lithium permselectivity $S_{Li/X}$ (•, measured), partitioning selectivity $S^{\alpha}_{Li/X}$ (○, measured), and mobility selectivity $S^{D}_{Li/X}$ (△, calculated based on the solution diffusion framework where $S_{Li/X} = S^{\alpha}_{Li/X} \times S^{D}_{Li/X}$) versus A) nickel, B) magnesium, and C) sodium in 4-vinylpryidine-containing membranes. Each ion pair is shown as an individual plot with ligand content (monomer mol %) on the x-axis. Error bars represent ± one standard deviation from triplicate experiments. Linear regressions of the logarithms of selectivities with ligand content (10-50 mol%) are shown as dashed

lines; statistically significant relationships are annotated based on F-tests (* $p \leq 0.05$; ** $p \leq 0.01$; *** $p \leq 0.001$).

In addition to identifying significant permselectivity trends with ligand content, we aimed to elucidate the mechanistic causes of these trends. To better understand the selectivity mechanisms in these ligand-functionalized membranes, we invoke the solution-diffusion framework that describes ion transport as sequential steps of (1) partitioning into the membrane (solubility) and (2) migrating through the membrane (diffusion). In this framework, permeability (P_i) is therefore described as the product of the ion partition (K_i) and diffusion (D_i) coefficients: $P_i \equiv K_i \times D_i$ [13,20,21,24]. By this same framework, overall permselectivity can therefore be decomposed into a partitioning selectivity ($S_{X/Y}^{\alpha}$) and a mobility selectivity ($S_{X/Y}^{D}$) [13]:

$$S_{X/Y} \equiv \frac{P_X}{P_Y} = \frac{K_X D_X}{K_Y D_Y} = \left(\frac{K_X}{K_Y}\right) \times \left(\frac{D_X}{D_Y}\right) = S_{X/Y}^{\alpha} \times S_{X/Y}^{D} \quad \text{(Eq 6)}$$

Thus, we supplemented our permselectivity measurements with sorption experiments to measure partitioning selectivity and facilitate calculation of mobility selectivity. For lithium/nickel separation across the pyridine membranes, we observed an inverse relationship between partitioning selectivity and overall permselectivity with ligand content (Fig. 4A). Although Li^+/Ni^{2+} permselectivity only increased by a factor of 3.3 from 0 to 50 mol% pyridine content, the Li^+/Ni^{2+} partitioning selectivity measured from sorption experiments decreased by a factor of 28. Consequently, the observed increase in Li^+/Ni^{2+} permselectivity with increasing pyridine content implies that Li^+/Ni^{2+} mobility selectivities increase by two orders of magnitude to outweigh the inverse partitioning selectivity trend. These observations are in agreement with prior theory and computation work asserting that mobility selectivity dominates partitioning selectivity in overall permselectivity trends for ligand-functionalized hydrogel membranes [21,44]. For example, one ion permeability model developed as a function of ion-ligand binding affinity predicted that mobility reductions outcompete partitioning enhancements at higher ion-membrane affinities, leading to an overall reduction in ion permeability with increasing ion-ligand binding affinity [21]. By analogy for the separation of two ions with different ion-ligand affinities, mobility selectivity (favoring transport of the low-affinity ion) is also expected to outweigh partitioning selectivity (favoring the high-affinity ion) in the determination of overall permselectivity. In the case where the ion-ligand affinity of the high-affinity ion increases while the other remains constant (e.g., increasing Ni^{2+}-pyridine affinity with membrane pyridine content and constant Li^+-pyridine affinity), this theory also predicts an increase in permselectivity of the lower-affinity ion (e.g., Li^+) due to mobility selectivity increasing more than partitioning selectivity decreases.

For Li^+/Mg^{2+} and Li^+/Na^+ separations, overall permselectivities were approximately constant across pyridine contents, averaging $S_{Li/Mg}$ = 8.6 ± 0.5 and $S_{Li/Na}$ = 1.14 ± 0.01. Still, the decline in Li^+/Mg^{2+} partitioning selectivity with pyridine content suggests that the corresponding Li^+/Mg^{2+} mobility selectivity trend must oppose it to result in the constant overall permselectivity (Fig. 4B). This trade-off in partitioning and mobility selectivities further confirms prior ligand-functionalized membrane transport theory and experimental observations [12,13,21]. In the case of Li^+/Na^+ separations, no significant trends were observed for overall partitioning selectivity nor its constituent partitioning and mobility selectivities with ligand content due to similar, weak Li^+-pyridine and Na^+-pyridine interactions (Fig. 4C).

Our findings experimentally demonstrate the dominant role of mobility selectivity, in agreement with prior work asserting that mobility effects outcompete partitioning effects in overall permselectivity, leading to higher permselectivity of the lower-affinity ion [21]. While prior efforts to tune the difference in ion-ligand affinity between two ions have largely focused on changing ligand identity, we show that similar effects can be achieved via changes in ligand content. The increase in permselectivity of the lower-affinity ion with increasing ligand content demonstrates that ligand content is a critical parameter for predicting ion transport. While previous literature considers homogeneous ion-ligand binding affinity among other parameters to predict ion permeability and permselectivity in ligand-functionalized membranes [21], we demonstrate that a constant homogeneous ion-ligand binding affinity does not capture the observed transport dependence on ligand content. Again, we postulate that higher ligand content may facilitate stronger multidentate ion-ligand interactions that are otherwise infeasible at lower contents due to steric hindrance within the membrane. Ligand content is therefore a critical variable for tuning membrane permselectivity between one ion capable of multidentate interactions (affinity and permeability influenced by ligand content) and another monodentate-coordinating ion (affinity and permeability independent of ligand content). At the same time, the competing mobility and partitioning trends observed with ligand content may suggest a fundamental limitation of ligand content (or more broadly, coordination chemistry interactions) for ion-ion separations.

3.4 Ligand-induced diffusive ion mobility limitations are maintained under electromigration

In Sections 3.2 and 3.3, the highest Li^+/X permselectivity was measured against nickel in the 50 mol% VP membrane because of strong Ni^{2+}-pyridine interactions hindering nickel transport and weak Li^+-pyridine interactions. In this monovalent (Li^+) versus divalent (Ni^{2+}) separation case, an additional fundamental question arises regarding the impact of diffusion versus electromigration driving force on permselectivity. Neglecting convective transport and assuming constant ion partition coefficients,

diffusivities, and interfacial solution concentrations, the Nernst-Planck equation would predict that divalent nickel would experience a greater permeability enhancement than monovalent lithium with increasing applied potential, and that Li^+/ Ni^{2+} permselectivity would consequently decline by a factor of 2 as electromigration becomes dominant compared to diffusive transport (Equation S1-S3) [28].

To advance understanding and rational design of ion transport in ligand-functionalized membranes, we varied the applied potential in an electrodialysis system to investigate whether permselectivity trends with driving force follow these Nernst-Planck expectations. We measured Li^+/Ni^{2+} permselectivity in a single electrodialysis stack with the 50 mol% VP membrane under a range of applied potentials (chronoamperometry plots shown in Fig. S7). The membranes were pre-soaked in the feed solution to eliminate the nickel sorption period in the experiment, which resulted in some initial nickel leaching into the permeate solution at the start of the experiments. 0.1 M H_2SO4 was used as electrolyte to mimic the application of lithium recovery from battery cathode active material leachate, which is acidic and commonly contains both lithium and nickel [45]. Diffusive Li^+/Ni^{2+} permselectivity was slightly reduced from an average of $S_{Li/Ni} = 12.7 \pm 2.7$ under the original circumneutral conditions (nanopure water permeate) to $S_{Li/Ni} = 4.7 \pm 0.8$ at pH 0.7 (0.1 M H_2SO4 permeate). Under these acidic conditions, membrane water uptake was found to rise by 28%, which may be due to protonation of the pyridine functional group (pKa 5.23 [46]). The resulting higher water volume fraction in the membrane caused a slight increase in average diffusive lithium permeability (1.9×). Average diffusive nickel permeability increased by a larger factor (5.1×) due to the enhanced mobility from reduced nickel-pyridine/pyridinium coordination in addition to the increased water volume fraction.

Surprisingly, Li^+/Ni^{2+} selectivity trends with applied potential were found to oppose the Nernst-Planck expectations. In our experiments, lithium transport across the 50 mol% VP membrane was more positively correlated with applied potential than nickel transport (Fig. S8A-B). Due to initial nickel leaching from the feed-soaked membranes and a decline in current (related to a decline in total ion transport) over the course of the constant-potential experiments, constant permeabilities could not be measured for lithium and nickel. Instead, the molar ratio of lithium to nickel in the permeate chamber normalized by the initial molar ratio in the feed chamber was used as a proxy for Li^+/Ni^{2+} permselectivity over time (Fig. 5). At all potentials, this selectivity proxy ratio of lithium to nickel in the permeate chamber increased over time due to initial leaching of the preferentially sorbed nickel from the membrane that was quickly superseded by a lower rate of sustained nickel transport (Fig. S8B). Consequently, the lithium to nickel molar ratios plateau over time as electromediated-ion transport overtakes initial ion leaching. Irrespective of the time-variant behavior, higher potentials generally achieved higher lithium transport and higher Li^+/Ni^{2+} molar ratios in the permeate chamber throughout the 24 h experiment. At the final timepoint, the Li^+/Ni^{2+} permeate ratio

was approximately 3× higher in the highest potential (6.5 V) experiment compared to the diffusive experiment (0 V). This trend in increasing Li^+/Ni^{2+} molar ratios with increasing applied potential is opposite of the expectations from the Nernst-Planck equation, which would instead predict a Li^+/Ni^{2+} selectivity reduction from the diffusive (0 V case) by up to a factor of 2× (Fig. 5).

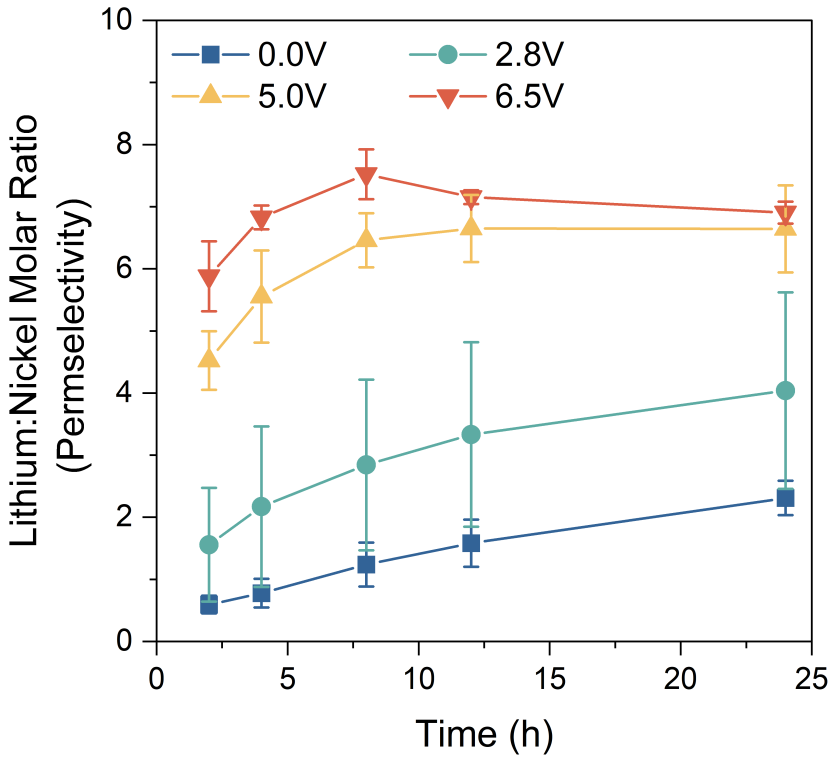

Fig. 5. Molar ratio of lithium to nickel concentrations in the permeate chamber over time for 4-chamber electrodialysis experiments operated at constant potentials of 0.0 V (diffusive case), 2.8 V, 5.0 V, and 6.5 V over 24 hours. Error bars represent ± one standard deviation from triplicate experiments.

Previous studies on ion exchange membranes have shown direct correlation of monovalent/divalent selectivities with applied potential and attributed this relationship to more extreme boundary layer transport limitations at higher applied potentials [47–51]. As boundary layer transport becomes rate-limiting, multivalent ion depletion in the boundary layer and higher aqueous diffusivities of monovalent ions are reasoned to lead to enhanced monovalent partitioning and permselectivity [47–51]. In our work, we do not observe the partitioning trends characteristic of boundary-layer nickel depletion. The post-electrodialysis test membranes were desorbed in nitric acid to characterize lithium and nickel sorption following the same

desorption procedure applied for partitioning selectivity measurements (Section 2.3). The Li^+/Ni^{2+} partitioning selectivity in the diffusive case with 0.1 M H_2SO_4 permeate ($S^{\alpha}_{Li/Ni}$ = 0.32 ± 0.28) was slightly higher than what was previously measured under diffusion with nanopure water permeate ($S^{\alpha}_{Li/Ni}$ = 0.11 ± 0.04), suggesting that the acidic environment impedes nickel-pyridine coordination and therefore enhances the Li^+/Ni^{2+} ratio within the membrane (though nickel sorption still remains preferential, i.e., $S^{\alpha}_{Li/Ni} < 1$). Under applied potentials, the Li^+/Ni^{2+} sorption selectivities were 3.0 to 4.5× lower ($S^{\alpha}_{Li/Ni}$ = 0.071 ± 0.001 to 0.11 ± 0.08) than in the diffusive case (Fig. 6). The reduction in lithium/nickel partitioning selectivity upon introduction of an applied potential was primarily due to an increase in nickel sorption in the membrane rather than a decrease in lithium sorption, suggesting that boundary layer depletion of nickel is not the cause of the Li^+/Ni^{2+} selectivity enhancement at higher potentials. Rather, these results support that while nickel still preferably partitions into the membrane, the nickel-membrane coordination remains sufficiently strong to hinder nickel mobility across the range of applied potentials studied (up to 6.5 V).

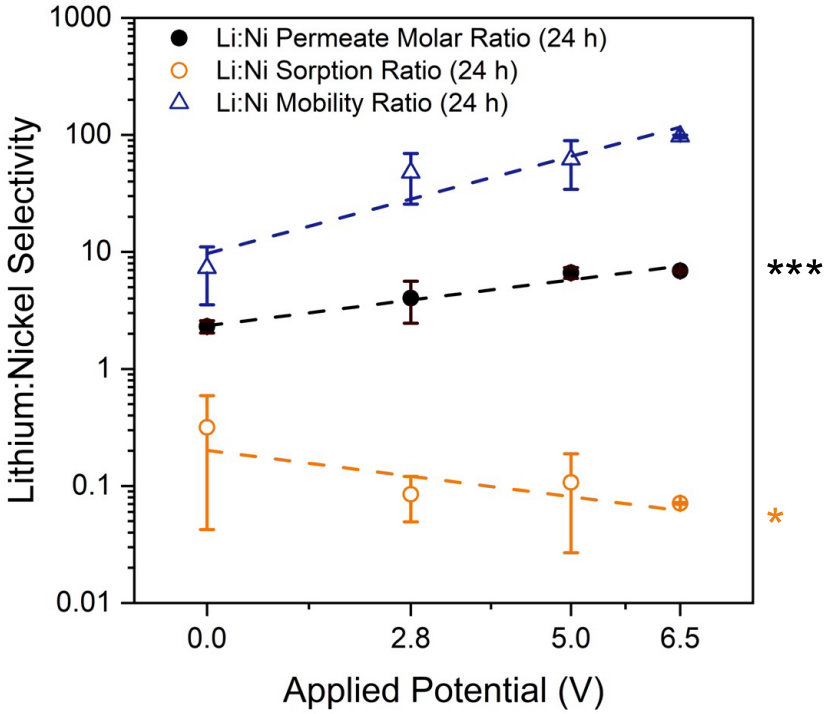

Fig. 6. Lithium/nickel permselectivity $S_{Li/Ni}$ (•, measured by the molar ratio of ions in the permeate chamber), partitioning selectivity $S^{\alpha}_{Li/Ni}$ (○, measured by the molar ratio of sorbed ions in the

membrane), and mobility selectivity $S^{D}_{Li/Ni}$ (▵, calculated based on the solution diffusion framework where $S_{Li/Ni} = S^{\alpha}_{Li/Ni} \times S^{D}_{Li/Ni}$) at 24 hours. Error bars represent ± one standard deviation from triplicate experiments. Linear regressions of the logarithms of selectivities with applied potential are shown as dashed lines; statistically significant relationships are annotated based on F-tests (* $p \leq 0.05$; ** $p \leq 0.01$; *** $p \leq 0.001$).

This finding is promising for the development of ligand-functionalized ion-selective electrodialysis membranes; it demonstrates that permselectivity for the low-affinity ion (e.g., lithium) may be maintained or even improved with applied potential if coordination with the high-affinity ion (e.g., nickel) is sufficiently strong relative to the electromigratory driving force. As a result, simultaneous improvements in productivity and selectivity can be achieved with an electric potential driving force. In the context of membrane process design, the departure of these selectivity results from diffusive results and expected Nernst-Planck trends motivate membrane testing under application conditions as critical for realistic estimates of ion-ion permselectivity. Such experiments can elucidate ligand-speciation effects, solution mass transport limitations, and the effects of competition between ion-ligand coordination and driving force.

4 Conclusions

In the development of ligand-functionalized membranes for ion-ion separations, few studies have systematically investigated the effect of fine-tuning membrane composition beyond ligand chemistry on separation performance. In this work, we fill this knowledge gap by synthesizing a library of acrylic acid- and pyridine-functionalized membranes and measuring ion permeabilities and permselectivities to provide valuable insights on the variable effects of ligand content on ion-ion permselectivity.

Specifically, we observe order-of-magnitude changes in ion permeability with increasing membrane ligand content for ions known to form multidentate ion-ligand complexes. In contrast, the permeabilities of weaker, monodentate-coordinating ions were relatively independent of ligand content. These results highlight ligand content as a critical variable for tuning the permselectivity between one ion capable of strong, multidentate interactions whose affinity and permeability are influenced by ligand content and another weak, monodentate-coordinating ion whose affinity and permeability are independent of ligand content. In the context of membrane design, where ligand selection is primarily informed by homogeneous ion-ligand binding affinities, our experimental results underscore the importance of considering the ligand content required to leverage strong, multidentate complex formation; changing a

ligand's content within a membrane may have just as substantial impacts on ion permselectivity as changing the ligand chemistry entirely.

The influence of driving force on membrane performance is another critical yet understudied parameter in membrane-based ion separations. Electrodialysis with 50 mol% VP membrane demonstrated simultaneous improvement in lithium recovery and Li^{+}/Ni^{2+} selectivity with applied potential, opposite of expectations from the valence-proportional electromigration term in the classical Nernst-Planck equation. While the observed trends followed previous reports of boundary layer mass transport limitations, partitioning selectivities suggest that preferential partitioning of nickel occurs at high potentials and that additional ligand-induced membrane transport limitations still exist to hinder nickel transport. These results emphasize the need for preliminary membrane testing under various driving force conditions (e.g., diffusion and applied potential) to robustly assess a membrane's performance potential for an application of interest.

Throughout this study, our experimental results support previous assertions that strong competing ion complexation can be used to achieve high permselectivity of a non-complexing ion [21]. Future work may include the study of additional ion-ligand combinations spanning a wider range of binding affinities to expand the experimental data set relating ion-selective membrane structure and performance. Considering different regimes of ion-ligand binding affinities and extension to surface-functionalized versus bulk-functionalized membranes may help explain some of the contrasting results reporting high permselectivity of the complexing ion in literature. Simultaneous work by theorists and computationalists to incorporate ligand content and driving force effects on (1) effective ion-membrane affinity and (2) ion-ion permselectivity would enhance existing ion transport models. We encourage further studies on the effect of electric fields on ion sorption selectivity in membranes, including but not limited to the study of ligand speciation and valence effects. Such models could help guide rational design and development of improved ion-selective ligand-functionalized membranes.

5 Acknowledgements

This work was supported by the Stanford Graduate Fellowship, the Stanford StorageX Initiative Seed Fund, the Toyota Electrochemical Society Young Investigator Fellowship, the Dreyfus Foundation Teacher-Scholar Award (TC-22-093), and Fundação de Amparo à Pesquisa do Estado de São Paulo and Capes (2019/11866-5, 2023/01032-5). ATR-FTIR characterization was performed at the Stanford Nano Shared Facilities (SNSF), supported by the National Science Foundation under award ECCS-2026822.

6 References

[1] R.M. DuChanois, N.J. Cooper, B. Lee, S.K. Patel, L. Mazurowski, T.E. Graedel, M. Elimelech, Prospects of metal recovery from wastewater and brine, Nat Water 1 (2023) 37–46. https://doi.org/10.1038/s44221-022-00006-z.

[2] Dean M. Miller, Kristen Abels, Jinyu Guo, Kindle S. Williams, Matthew J. Liu, William A. Tarpeh, Electrochemical Wastewater Refining: A Vision for Circular Chemical Manufacturing | Journal of the American Chemical Society, J. Am. Chem. Soc. (2023). https://doi.org/10.1021/jacs.3c01142.

[3] The Role of Critical Minerals in Clean Energy Transitions, International Energy Agency, 2022.

[4] A. Kumar, H. Fukuda, T.A. Hatton, J.H. Lienhard, Lithium Recovery from Oil and Gas Produced Water: A Need for a Growing Energy Industry, ACS Energy Lett. 4 (2019) 1471–1474. https://doi.org/10.1021/acsenergylett.9b00779.

[5] G.M. Geise, H.-S. Lee, D.J. Miller, B.D. Freeman, J.E. McGrath, D.R. Paul, Water purification by membranes: The role of polymer science, Journal of Polymer Science Part B: Polymer Physics 48 (2010) 1685–1718. https://doi.org/10.1002/polb.22037.

[6] M. Mulder, Basic Principles of Membrane Technology, Springer Netherlands, Dordrecht, 1996. https://doi.org/10.1007/978-94-009-1766-8.

[7] R.W. Baker, Membrane technology and applications, 3rd ed, John Wiley & Sons, Chichester, West Sussex ; Hoboken, 2012.

[8] O. Nordness, J.D. Moon, N. Marioni, E.S. Zofchak, P.M. Richardson, M.R. Landsman, L.E. Katz, C.J. Hawker, V. Ganesan, R.A. Segalman, R.J. Clément, Probing Water and Ion Diffusion in Functional Hydrogel Membranes by PFG-NMR, Macromolecules 56 (2023) 4669–4680. https://doi.org/10.1021/acs.macromol.3c00306.

[9] M. Heiranian, R.M. DuChanois, C.L. Ritt, C. Violet, M. Elimelech, Molecular Simulations to Elucidate Transport Phenomena in Polymeric Membranes, Environ. Sci. Technol. 56 (2022) 3313–3323. https://doi.org/10.1021/acs.est.2c00440.

[10] E.S. Zofchak, Z. Zhang, N. Marioni, H.S. Sachar, B.D. Freeman, V. Ganesan, Cation–polymer interactions and local heterogeneity determine the relative order of alkali cation diffusion coefficients in PEGDA hydrogels, Journal of Membrane Science 685 (2023) 121898. https://doi.org/10.1016/j.memsci.2023.121898.

[11] H. Fan, Y. Huang, N.Y. Yip, Advancing ion-exchange membranes to ion-selective membranes: principles, status, and opportunities, Front. Environ. Sci. Eng. 17 (2023) 25. https://doi.org/10.1007/s11783-023-1625-0.

[12] H.S. Sachar, E.S. Zofchak, N. Marioni, Z. Zhang, S. Kadulkar, T.J. Duncan, B.D. Freeman, V. Ganesan, Impact of Cation–Ligand Interactions on the Permselectivity of Ligand-Functionalized Polymer Membranes in Single and Mixed Salt Systems, Macromolecules 55 (2022) 4821–4831. https://doi.org/10.1021/acs.macromol.2c00543.

[13] E.S. Zofchak, Z. Zhang, B.K. Wheatle, R. Sujanani, S.J. Warnock, T.J. Dilenschneider, K.G. Hanson, S. Zhao, S. Mukherjee, M.M. Abu-Omar, C.M. Bates, B.D. Freeman, V. Ganesan, Origins of Lithium/Sodium Reverse Permeability Selectivity in 12-Crown-4-Functionalized Polymer Membranes, ACS Macro Lett. 10 (2021) 1167–1173. https://doi.org/10.1021/acsmacrolett.1c00243.

[14] R.M. DuChanois, M. Heiranian, J. Yang, C.J. Porter, Q. Li, X. Zhang, R. Verduzco, M. Elimelech, Designing polymeric membranes with coordination chemistry for high-precision ion separations, Sci. Adv. 8 (2022) eabm9436. https://doi.org/10.1126/sciadv.abm9436.

[15] R.M. DuChanois, L. Mazurowski, H. Fan, R. Verduzco, O. Nir, M. Elimelech, Precise Cation Separations with Composite Cation-Exchange Membranes: Role of Base Layer Properties, Environ. Sci. Technol. 57 (2023) 6331–6341. https://doi.org/10.1021/acs.est.3c00445.

[16] J. Li, H. Yi, M. Wang, F. Yan, Q. Zhu, S. Wang, J. Li, B. He, Z. Cui, Preparation of Crown-Ether-Functionalized Polysulfone Membrane by In Situ Surface Grafting for Selective Adsorption and Separation of Li^{+}, ChemistrySelect 5 (2020) 3321–3329. https://doi.org/10.1002/slct.201904836.

[17] C. Sheng, S. Wijeratne, C. Cheng, G.L. Baker, M.L. Bruening, Facilitated ion transport through polyelectrolyte multilayer films containing metal-binding ligands, Journal of Membrane Science 459 (2014) 169–176. https://doi.org/10.1016/j.memsci.2014.01.051.
[18] S.J. Warnock, R. Sujanani, E.S. Zofchak, S. Zhao, T.J. Dilenschneider, K.G. Hanson, S. Mukherjee, V. Ganesan, B.D. Freeman, M.M. Abu-Omar, C.M. Bates, Engineering Li/Na selectivity in 12-Crown-4–functionalized polymer membranes, Proc. Natl. Acad. Sci. U.S.A. 118 (2021) e2022197118. https://doi.org/10.1073/pnas.2022197118.
[19] W.G.B. Mandersloot, Preferential Ion Transport in Electrodialysis through Ion-exchange Resin Membranes, BCSJ 37 (1964) 1442–1448. https://doi.org/10.1246/bcsj.37.1442.
[20] S.J. Warnock, R. Sujanani, E.S. Zofchak, S. Zhao, T.J. Dilenschneider, K.G. Hanson, S. Mukherjee, V. Ganesan, B.D. Freeman, M.M. Abu-Omar, C.M. Bates, Engineering Li/Na selectivity in 12-Crown-4–functionalized polymer membranes, Proc. Natl. Acad. Sci. U.S.A. 118 (2021) e2022197118. https://doi.org/10.1073/pnas.2022197118.
[21] E.S. Zofchak, Z. Zhang, N. Marioni, T.J. Duncan, H.S. Sachar, A. Chamseddine, B.D. Freeman, V. Ganesan, Cation–Ligand Interactions Dictate Salt Partitioning and Diffusivity in Ligand-Functionalized Polymer Membranes, Macromolecules 55 (2022) 2260–2270. https://doi.org/10.1021/acs.macromol.2c00035.
[22] R. Wang, R. Duddu, S. Lin, Extended Donnan-Manning theory for selective ion partition and transport in ion exchange membrane, Journal of Membrane Science 681 (2023) 121782. https://doi.org/10.1016/j.memsci.2023.121782.
[23] E.-S. Jang, J. Kamcev, K. Kobayashi, N. Yan, R. Sujanani, T.J. Dilenschneider, H.B. Park, D.R. Paul, B.D. Freeman, Influence of water content on alkali metal chloride transport in cross-linked Poly(ethylene glycol) Diacrylate.1. Ion sorption, Polymer 178 (2019) 121554. https://doi.org/10.1016/j.polymer.2019.121554.
[24] E.-S. Jang, J. Kamcev, K. Kobayashi, N. Yan, R. Sujanani, T.J. Dilenschneider, H.B. Park, D.R. Paul, B.D. Freeman, Influence of water content on alkali metal chloride transport in cross-linked Poly(ethylene glycol) diacrylate.2. Ion diffusion, Polymer 192 (2020) 122316. https://doi.org/10.1016/j.polymer.2020.122316.
[25] E. Tsuchida, H. Nishide, Polymer effect in the chelate formation of macromolecules, Die Makromolekulare Chemie 14 (1985) 71–80. https://doi.org/10.1002/macp.1985.020141985107.
[26] L. Wu, C. Zhang, S. Kim, T.A. Hatton, H. Mo, T.D. Waite, Lithium recovery using electrochemical technologies: Advances and challenges, Water Research 221 (2022) 118822. https://doi.org/10.1016/j.watres.2022.118822.
[27] National Academies of Sciences, Engineering, and Medicine, A Research Agenda for Transforming Separation Science, The National Academies Press, Washington, DC, 2019. https://doi.org/10.17226/25421.
[28] H. Luo, W.-A.S. Agata, G.M. Geise, Connecting the Ion Separation Factor to the Sorption and Diffusion Selectivity of Ion Exchange Membranes, Ind. Eng. Chem. Res. 59 (2020) 14189–14206. https://doi.org/10.1021/acs.iecr.0c02457.
[29] J.D. Moon, R. Sujanani, Z. Geng, B.D. Freeman, R.A. Segalman, C.J. Hawker, Versatile Synthetic Platform for Polymer Membrane Libraries Using Functional Networks, Macromolecules 54 (2021) 866–873. https://doi.org/10.1021/acs.macromol.0c02414.
[30] C.-C. Yeh, A. Venault, Y. Chang, Structural effect of poly(ethylene glycol) segmental length on biofouling and hemocompatibility, Polym J 48 (2016) 551–558. https://doi.org/10.1038/pj.2016.5.
[31] H. Lin, E. Wagner, J. Swinnea, B. Freeman, S. Pas, A. Hill, S. Kalakkunnath, D. Kalika, Transport and structural characteristics of crosslinked poly(ethylene oxide) rubbers, Journal of Membrane Science 276 (2006) 145–161. https://doi.org/10.1016/j.memsci.2005.09.040.
[32] B. Nearingburg, A.L. Elias, Photopolymerizable sulfonated poly(ethylene glycol) proton exchange membranes for microfluidic and fuel cell applications, Journal of Membrane Science 389 (2012) 148–154. https://doi.org/10.1016/j.memsci.2011.10.024.

[33] H. Elliss, F. Dawson, Q. un Nisa, N.M. Bingham, P.J. Roth, M. Kopeć, Fully Degradable Polyacrylate Networks from Conventional Radical Polymerization Enabled by Thionolactone Addition, Macromolecules 55 (2022) 6695–6702. https://doi.org/10.1021/acs.macromol.2c01140.
[34] J. Kamcev, D.R. Paul, B.D. Freeman, Effect of fixed charge group concentration on equilibrium ion sorption in ion exchange membranes, J. Mater. Chem. A 5 (2017) 4638–4650. https://doi.org/10.1039/C6TA07954G.
[35] Predicting the Conductivity–Selectivity Trade-Off and Upper Bound in Ion-Exchange Membranes | ACS Energy Letters, (n.d.). https://pubs.acs.org/doi/full/10.1021/acsenergylett.4c00301 (accessed July 23, 2024).
[36] G.M. Geise, M.A. Hickner, B.E. Logan, Ionic Resistance and Permselectivity Tradeoffs in Anion Exchange Membranes, ACS Appl. Mater. Interfaces 5 (2013) 10294–10301. https://doi.org/10.1021/am403207w.
[37] E.R. Nightingale, Phenomenological Theory of Ion Solvation. Effective Radii of Hydrated Ions, J. Phys. Chem. 63 (1959) 1381–1387. https://doi.org/10.1021/j150579a011.
[38] H. Fan, Y. Huang, I.H. Billinge, S.M. Bannon, G.M. Geise, N.Y. Yip, Counterion Mobility in Ion-Exchange Membranes: Spatial Effect and Valency-Dependent Electrostatic Interaction, ACS EST Eng. (2022) acsestengg.1c00457. https://doi.org/10.1021/acsestengg.1c00457.
[39] NIST46, NIST (2013). https://www.nist.gov/srd/nist46 (accessed December 26, 2023).
[40] P.J. Proll, L.H. Sutcliffe, Dissociation constants of some inorganic acetates in anhydrous acetic acid, Trans. Faraday Soc. 57 (1961) 1078. https://doi.org/10.1039/tf9615701078.
[41] I. Despotović, Complexation of some alkali and alkaline earth metal cations by macrocyclic compounds containing four pyridine subunits – a DFT study, New J. Chem. 39 (2015) 6151–6162. https://doi.org/10.1039/C5NJ00459D.
[42] H. Nose, M.T. Rodgers, Influence of the d Orbital Occupation on the Structures and Sequential Binding Energies of Pyridine to the Late First-Row Divalent Transition Metal Cations: A DFT Study, J. Phys. Chem. A 118 (2014) 8129–8140. https://doi.org/10.1021/jp500488t.
[43] A.A. Uliana, N.T. Bui, J. Kamcev, M.K. Taylor, J.J. Urban, J.R. Long, Ion-capture electrodialysis using multifunctional adsorptive membranes, Science 372 (2021) 296–299. https://doi.org/10.1126/science.abf5991.
[44] R.S. Kingsbury, M.A. Baird, J. Zhang, H.D. Patel, M.J. Baran, B.A. Helms, E.M.V. Hoek, Kinetic barrier networks reveal rate limitations in ion-selective membranes, Matter 7 (2024) 2161–2183. https://doi.org/10.1016/j.matt.2024.03.021.
[45] K.H. Chan, M. Malik, G. Azimi, Separation of lithium, nickel, manganese, and cobalt from waste lithium-ion batteries using electrodialysis, Resources, Conservation and Recycling 178 (2022) 106076. https://doi.org/10.1016/j.resconrec.2021.106076.
[46] PubChem, Pyridine, (n.d.). https://pubchem.ncbi.nlm.nih.gov/compound/1049 (accessed July 10, 2024).
[47] J. Ying, M. Luo, Y. Jin, J. Yu, Selective separation of lithium from high Mg/Li ratio brine using single-stage and multi-stage selective electrodialysis processes, Desalination 492 (2020) 114621. https://doi.org/10.1016/j.desal.2020.114621.
[48] A.M. Mani, S. Chaudhury, G. Meena, Current Density Dependence of Transport Selectivity of Metal Ions in the Electrodriven Process across the Cation Exchange Membrane, J. Phys. Chem. B 127 (2023) 8879–8887. https://doi.org/10.1021/acs.jpcb.3c05051.
[49] A. Kitamoto, Y. Takashima, PREFERENTIAL ION TRANSPORT THROUGH ION EXCHANGE MEMBRANES BY ELECTRODIALYSIS, J. Chem. Eng. Japan / JCEJ 3 (1970) 54–62. https://doi.org/10.1252/jcej.3.54.
[50] Y. Kim, W.S. Walker, D.F. Lawler, Competitive separation of di- vs. mono-valent cations in electrodialysis: Effects of the boundary layer properties, Water Research 46 (2012) 2042–2056. https://doi.org/10.1016/j.watres.2012.01.004.

[51] X. Xu, Q. He, G. Ma, H. Wang, N. Nirmalakhandan, P. Xu, Selective separation of mono- and di-valent cations in electrodialysis during brackish water desalination: Bench and pilot-scale studies, Desalination 428 (2018) 146–160. https://doi.org/10.1016/j.desal.2017.11.015.